JOURNAL OF APPLIED ELECTROCHEMISTRY **28** (1998) 1113–1120

Characterization of zinc–nickel alloys obtained from an industrial chloride bath

G. BARCELÓ, E. GARCÍA, M. SARRET, C. MÜLLER*

Laboratori de Ciència i Tecnologia Electroquímica de Materials (LCTEM), Dpt. Química Física. Universitat de Barcelona, Martí I Franquès, 1, 08028-Barcelona, Spain

J. PREGONAS

PREMA S.A. Company. Benages 17, 08786-Capellades, Spain

Received 27 October 1997; accepted in revised form 10 March 1998

Zinc–nickel electrocoatings obtained from an industrial bath containing two additives were characterized by analysing their morphology, structure, microhardness, residual stress and corrosion resistance. Changes in deposit characteristics following the addition of saccharin were also studied. All coating, with or without saccharin, presented a good appearance, good mechanical properties and a high corrosion resistance. Moreover, by varying certain plating conditions it was observed that the deposits maintained their properties over a wide interval of experimental conditions, which suggests their suitability for use in batch bath.

Keywords: *zinc–nickel electrocoatings*, *characterization*, *electrochemical corrosion*, *residual stress*

1. Introduction

In recent years, several attempts have been made at preparing zinc coatings with high corrosion resistance. In so doing, zinc alloys with the group 8 metals have been developed [1–3] and, among theses, zinc–nickel alloys have received most attention because of their high degree of corrosion resistance and their mechanical properties.

Although slight variations have been reported, it is accepted that the highest corrosion resistance of zinc–nickel alloys can be obtained with a nickel content in the 10–15% range and various electrolytes have been reported as depositing Zn–Ni coatings with this composition [4–8]. In previous studies of this group, zinc–nickel electroplates with the desired composition and good corrosion behaviour were obtained from an acid bath containing a high concentration of NH_4Cl [9]. However, ecological considerations have led us to design a new plating bath without complexing agents to obtain zinc–nickel coatings in a batch bath and with commercially attractive properties. Our first objective is to characterize the zinc–nickel alloys obtained with this new acid bath by analysing their composition, morphology, structure, corrosion resistance and certain mechanical properties (microhardness, residual stress). Since most of the characteristics of the electrocoatings are structure dependent and the structure, in turn, is determined by the plating conditions, our second objective is to attempt to establish the relationship between electrodeposition parameters, structural properties and functionality.

* To whom correspondence should be addressed.

2. Experimental details

The zinc–nickel coatings were deposited under galvanostatic conditions at 200 A m^{-2} up to a constant thickness of 10 μm, using a chloride industrial bath (1.0 mol dm^{-3} in Zn^{2+} and 0.25 mol dm^{-3} in Ni^{2+}) at pH 5.2 and 28 °C. The basic electrolyte contained two additives (7.0 g dm^{-3} of a tensioactive and 0.2 g dm^{-3} of an aromatic aldehyde) and saccharin (2.0 g dm^{-3} was added in a number of cases to analyse the effect of the latter on deposit properties. In addition, alloys obtained with small variations in these basic conditions ($\pm 10\%$ of temperature, pH, bath concentration) were also characterized to determine the properties of the alloys that might be obtained under these conditions in industrial plant. A range of current densities in the interval 50–500 A m^{-2} and of deposit thicknesses, from 5 to 30 μm, were used in studying the influence of these parameters on the characteristics of the alloys.

The experimental set-up for the plating processes was as described in [9]. After deposition, some of the coatings were chromated by immersion for 25 s at 25 °C in a chromating solution, before being rinsed in deionised water and dried in warm air.

Deposit morphology was examined by optical microscopy (OM) and scanning electron microscopy (SEM) and film composition by atomic absorption spectrophotometry and XPS techniques. X-ray diffractograms were obtained on a Bragg–Brentano Siemens D500 diffractometer using CuK_α radiation (0.1542 nm) and the analysis of texture and the determination of microdeformations and the size of the coherent diffracting domains (CDD) were carried

0021-891X

out. These parameters were calculated by analysing the broadening of the X-ray diffraction lines. With this method the profile of the diffraction line is described by a Voigt function, representing a convolution of the Cauchy and Gauss functions, where it is assumed that the broadening due to the small CDD is according to the Cauchy-type only, while that due to the microdeformations is of the Gaussian-type [10, 11].

The diffractometer described above and a texture goniometer Philips MRD were used in analysing the residual stress of the coatings, using the $\sin^2\Psi$ method [12]. Thus, the stress, σ_ϕ, can be obtained from the relationship:

$$\frac{d_{\phi\Psi} - d_o}{d_o} = \frac{1+\nu}{E}\sigma_\phi \sin^2\Psi - \frac{\nu}{E}(\sigma_1 + \sigma_2) \qquad (1)$$

where $d_{\phi\Psi}$ and d_o are the stressed and unstressed lattice parameters, σ_1 and σ_2 are the principal stresses, ν is Poisson's ratio and E is Young's modulus. This equation predicts a linear variation d against $\sin^2\Psi$ from which slope the stress σ_ϕ can be derived if d_o, ν and E are known. Since d_o may not be readily available in practice, the lattice spacing measured at $\Psi = 0$ is usually substituted for d_o. As was performed elsewhere [13], ν and E were calculated in accordance with the percentage of pure Zn and Ni values or with Young's modulus given in the bibliography for zinc–nickel alloys 12% Ni [14].

The microhardness of the films was measured with a Matsuzawa MXT equipped with a Vickers diamond indenter and using a load of 50 g. In taking these measurements, the thickness of the deposits was constant at 30 μm, so as to obtain a value uninfluenced by the substrate.

Corrosion behaviour was studied by the salt-spray test (ASTM conditions) and by electrochemical techniques. These measurements were performed with EGG 273 and Schlumberger 1287–1255 systems. The cell was an EGG corrosion cell (exposed area 1 cm^2) and the test environment was a 5% NaCl solution in aerated conditions. At immersion, E_{corr} was measured until no further change was observed and then, the corrosion data were recorded. Impedance measurements were carried out in the frequency range 10^4–10^{-4} Hz. In a previous study [15], it was observed that for chromated zinc coatings more reproducible data were obtained after seven days of ageing at room temperature and so, the same period was respected here before analysis of the zinc–nickel chromated deposits was undertaken.

3. Results and discussion

Figure 1 shows the effect of current density on alloy composition and current efficiency, together with the polarization curve for the basic bath. The addition of saccharin promoted a slight positive shift in the deposition potentials, but the composition and efficiency remained practically unmodified. Figure 1, illustrates that these baths provided a wide interval of current densities with a constant composition of the coatings, between 10 and 14% Ni, depending on the plating temperature, pH and additive concentrations. On the other hand, the composition depth profile of the deposits showed that the alloys were uniform in composition (Fig. 2), unlike observations made with zinc–nickel alloys of the same global composition obtained from an ammonium bath, where the percentage of nickel of the coatings decreased with the deposition time [9, 16]. Moreover, here the composition of the alloys as determined by ESCA coincided with that obtained by absorption spectrophotometry and no preferential sputtering of zinc was observed. Preferential sputtering has been observed elsewhere when the alloy constituents differ appreciably in their heats of sublimation [17] but it is clear that the preferential sputtering of zinc is not merely a conse-

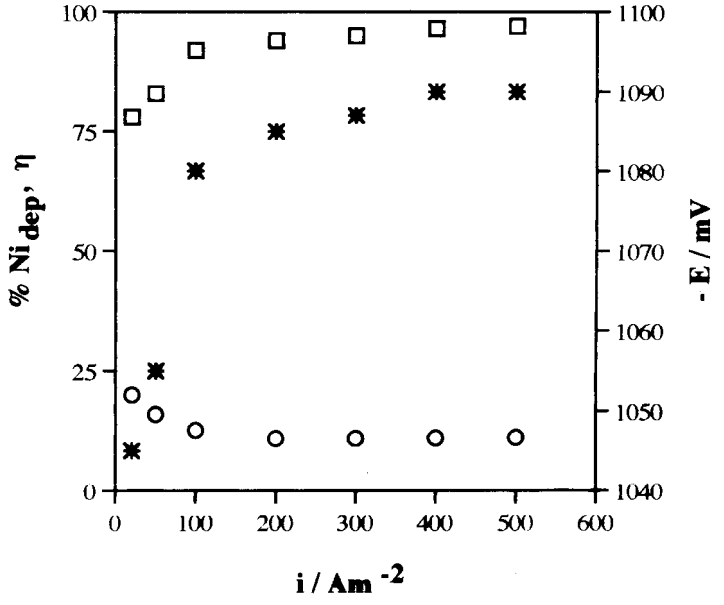

Fig. 1. Effect of current density on nickel content of deposits (○), on current efficiency (η) for alloy deposition (□) and polarization curve (*) during the deposition process.

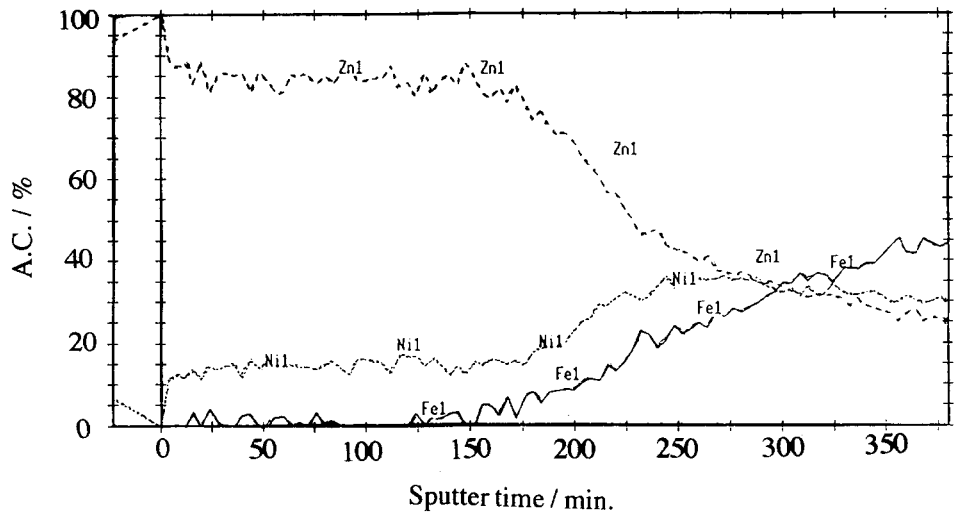

Fig. 2. ESCA depth profile of a Zn–Ni alloy containing a 12% Ni.

quence of the difference between the sublimation heats of Zn and Ni and that other factors, such as composition or structure, need to be considered.

When using the basic electrolyte or upon adding saccharin, bright homogeneous deposits were obtained with current densities up to 700 A m^{-2}. The surface morphology of the deposits was examined by SEM and optical microscopy. The coatings obtained under different conditions were highly similar: they consisted of nodular grains which were not very uniformly distributed (Fig. 3) and, as usual, those obtained at low current densities presented larger grains. The most surprising fact was observed in the cross-section of the electroplates obtained with the lowest Ni^{2+} concentration and saccharin, where many fissures that opened up near the substrate boundary were observed (Fig. 4). After the chromating process, the coatings showed a smoother surface and in some cases, a network of microcracks, characteristic of the passivation layer, was observed.

The microstructure of the coatings was studied by diffractometric analysis. X-ray diffractograms of the alloys with the basic bath showed the presence of γ-phase with the highest reflection intensity corresponding to the (3 3 0) and (6 0 0) preferential orientations (Fig. 5a). An accurate analysis of the diffractometric peaks revealed the presence of small amounts of η-phase, as corresponds to a nickel content of 10–14% (the percentage of nickel of a pure γ-phase should be 17.8% by mass). The addition of saccharin did not result in any major texture change, but an increase in the intensity of the peaks corresponding to the (2 2 2) and (4 4 4) orientations was observed (Fig. 5b). The chromating film scarcely modified the diffractometric response of the deposits, although in the deposits obtained with saccharin, the peaks corresponding to the (2 2 2) or (4 4 4) orientations were seen to disappear (Fig. 5c). This result would seem to indicate that these crystallographic planes were mainly situated near the deposit surface

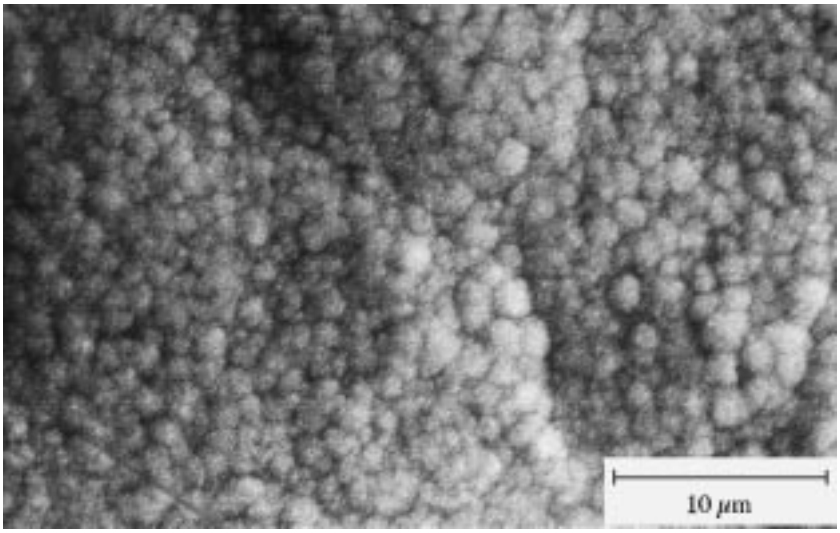

Fig. 3. SEM picture of a Zn–Ni alloy obtained without saccharine at 200 A m^{-2}.

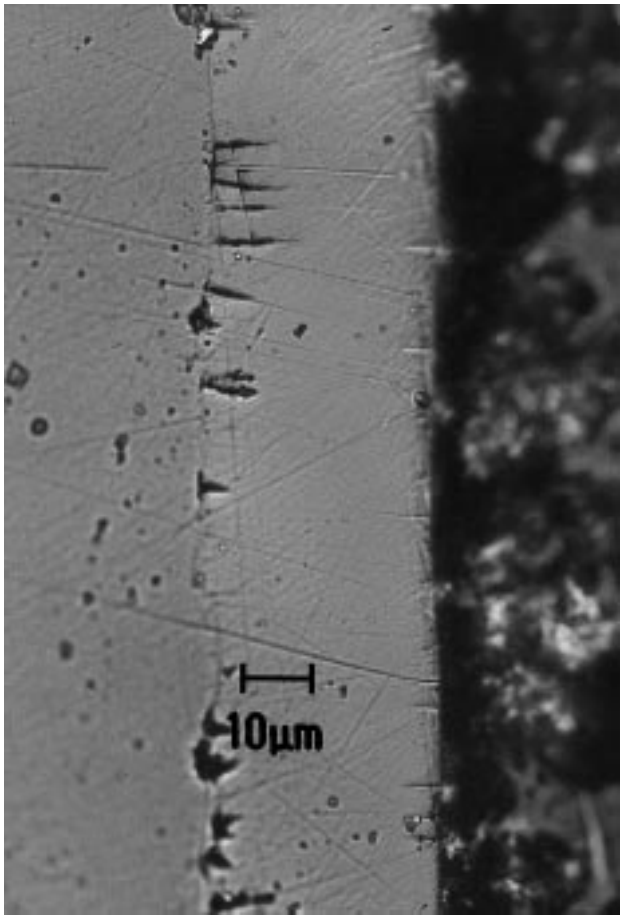

Fig. 4. Cross-section of a Zn–Ni alloy obtained with saccharine at 200 A m^{-2}.

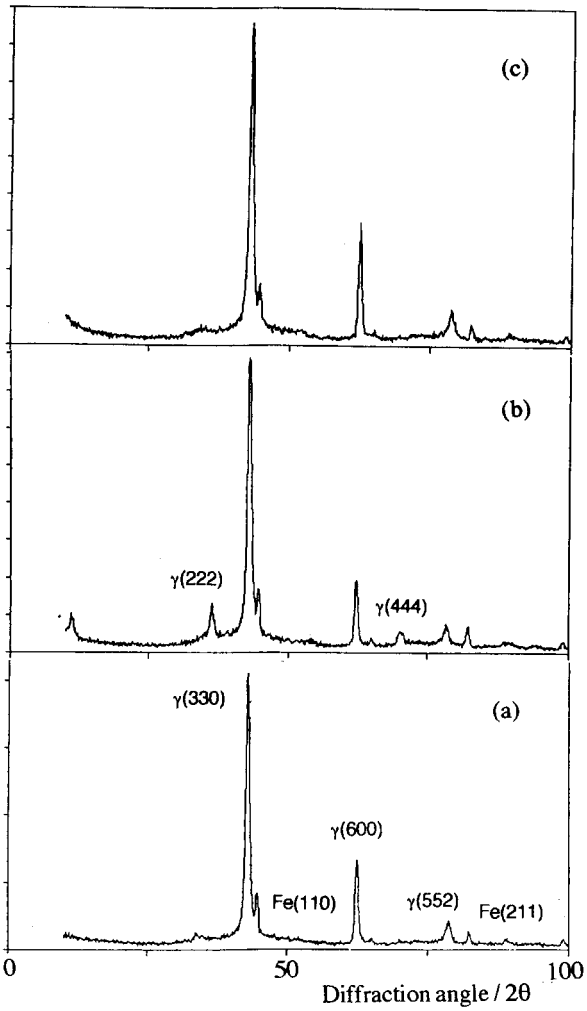

Fig. 5. X-ray diffractograms for Zn–Ni deposits obtained: (a) with the basic bath, (b) with saccharine, (c) with saccharine and passivated.

and they were preferentially dissolved during the alloy oxidation promoted by the chromating process.

To study the evolution of the preferred orientation with the current density and deposit growth, the texture coefficient T_{hkl} was calculated for the various (hkl) reflections [18]:

$$T_{hkl} = \frac{I_{hkl}/I^{o}_{hkl}}{\left((1/n)\sum_{n}(I_{hkl}/I^{o}_{hkl})\right)} \qquad (2)$$

where I_{hkl} is the intensity of the diffractometric peak, I^{o}_{hkl} is the standard random peak intensity and n is the number of measured peaks. When the texture coefficient calculated for the different reflections was plotted as a function of the current density, no changes in the texture were observed. However, when plotting T_{hkl} against deposit thickness the coating tended to the (6 0 0) orientation as the thickness increased and this increase in the (6 0 0) intensity occurred at the expense of the (3 3 0) reflection.

The determination of the lattice parameter (a), microdeformations (e) and the size of the coherent diffracting domains (CDD) was mainly performed from the peak corresponding to the (6 0 0) orientation. As seen in Fig. 5, the peak corresponding to the (3 3 0) orientation overlapped that corresponding to the (1 1 0) orientation of the iron substrat and it also had a small contribution of the (1 0 1) orientation of η-phase and so that deconvolution was needed. With some deposits it was verified that after the deconvolution process the results obtained from the (3 3 0) and (6 0 0) orientations were highly similar and so this latter orientation was used in most cases to determine the aforementioned parameters.

Figure 6 shows the influence of current density on a, CSD, and e for nonchromated alloys obtained with the basic bath. As usual, an increase in current density led to a fall in both grain size and the size of the coherent diffracting domains, but concurrent to this the crystals grew faster, with a significant increase in the number of faults, dislocations and microstrains. However, the microdeformation values obtained for these coatings were lower than those determined for other electrodeposits using the same XRD method [19]. On the other hand, the lattice parameter also increased with current density, but this was mainly due to the variations in alloy composition (Fig. 1). As mentioned above, these alloys were constituted of γ-phase and included some excess of zinc. The diffractograms indicated that, although they contained some η-phase, most of the zinc was included in the γ-phase lattice. Since zinc atoms are larger than those of nickel ($r_{Zn} = 1.37$ Å, $r_{Ni} = 1.25$ Å), the interca-

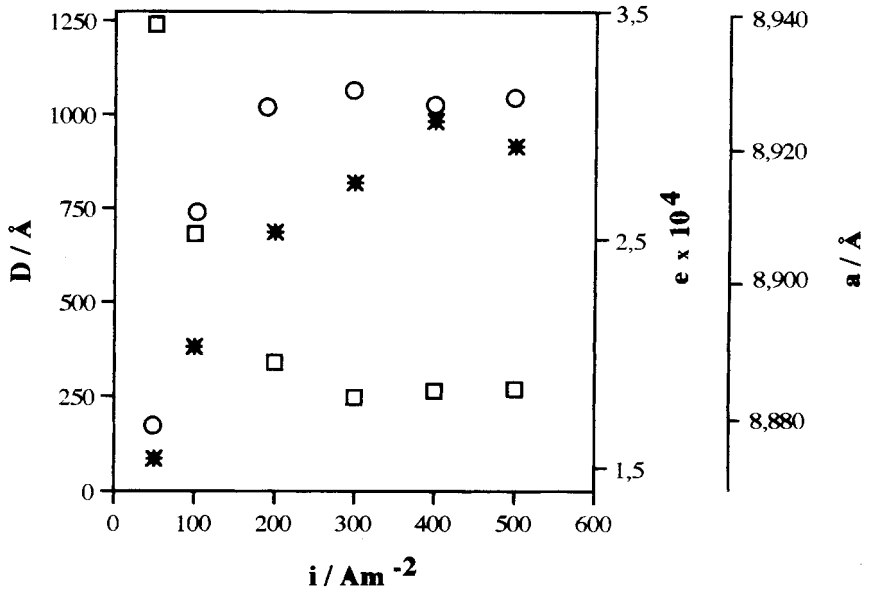

Fig. 6. Effect of current density on coherent scattering domains (□), microdeformations (*) and lattice parameter (○) of Zn–Ni alloys deposited from the basic bath.

lation of zinc into the f.c.c. lattice of γ-phase led to an increase in the lattice parameter. Finally, neither the lattice parameter nor the size of the coherent diffracting domains and microdeformations varied appreciably with the deposit thickness.

The residual stress of the coatings was determined using the $\sin^2\Psi$ method. Figure 7 shows the d against $\sin^2\Psi$ plots obtained for the (6 0 0) family of planes of a deposit obtained with the basic bath. The oscillatory behaviour observed in these plots was also observed in zinc coatings obtained with a chloride bath that contained a similar family of additives [15]. Such oscillations have been explained by taking into consideration the superposition of strong gradients and shear stresses normal to the surface or the anisotropy in the X-ray elastic constants [12] but an average residual stress can be estimated by considering the average slope of the plots. With this procedure, the residual stress calculated for the alloys obtained from the basic bath was of 204 ± 24 MPa, which agrees with the values reported for zinc–nickel alloys of this composition [3]. On the other hand, the variation in stress with deposit thickness appeared to be very small, in contrast to the effects observed elsewhere [12], decreasing with an increase in current density and becoming constant at 200 A m^{-2}. Finally, it must be mentioned that small variations in the plating conditions had no great influence on the stress of the coatings, except for the concentration of the tensioactive; a decrease in the concentration of this compound always generated an increase in the stress level.

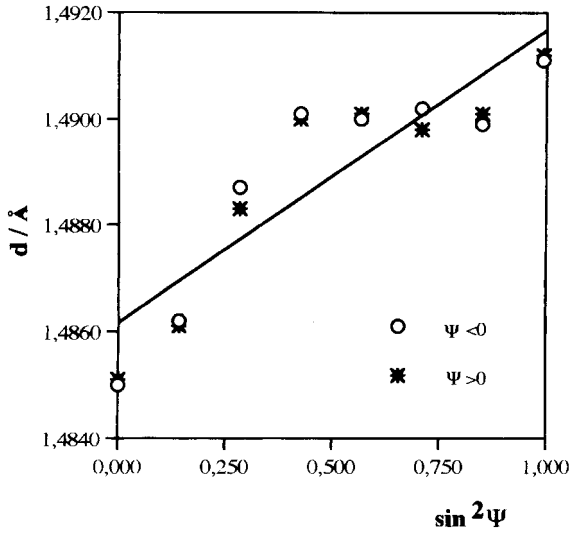

Fig. 7. Variation in the (6 0 0) lattice parameter with $\sin^2\Psi$ for Zn–Ni deposits obtained with the basic bath.

The microhardness of the 30 μm thick alloys obtained with the basic bath was measured with the Vickers method. It was observed that the values were mainly dependent on the composition of the alloy, included in the interval 393–472 HV for alloys containing 11–14% Ni, obtained under different experimental conditions.

Table 1 summarizes the influence of saccharin on the various characteristics of the zinc–nickel coatings. The addition of saccharin to the plating bath scarcely modified the residual stress level, except when fissures were observed in the cross section of the coatings. When this was the case, a very low value (67 ± 11 MPa) was obtained and this would seem to be related to relaxation during the deposition of the first layers of the alloy. Saccharin is a commun additive used in reducing stress in Ni electrodeposits and it is generally accepted that the decrease in residual stress is due to the restriction of lateral growth and the inhibition of coalescence of separate islands in the initial deposition stages [21]. As previously observed with Zn electrodeposits [15], with this Zn–Ni alloy the influence of saccharin on the residual

Table 1. Lattice parameter (a), size of the coherently diffracting domain (CDD), microstrain (e), microhardness and residual stress for Zn–Ni coatings 11% Ni obtained at 200 A m^{-2} (Cr: passivated)

Plating bath	*a* /Å	*CDD* /Å	$e \times 10^4$	*Microhardness* /HV	*Residual stress* /MPa
Basic	8.925	343	2.6	393	253 ± 24
Basic + sacch.	8.941	279	1.6	362	204 ± 19
Basic (Cr)	–	249	7.7	472	297 ± 18
Basic + sacch. (Cr)	–	258	2.8	454	364 ± 26

stress was not as great as that observed in Ni deposits. The alteration of microdeformations and CDD proceeded simultaneously with changes in residual stress, and no major differences were observed on adding saccharin. The same behaviour was observed with microhardness, except in those electroplates that developed fissures; in this case the presence of these cracks lowered microhardness by up to 215 HV.

The influence of the chromating process on these properties of the coatings is also summarized in Table 1. As expected, the passivation film increased the microhardness and residual stress of the deposits [22]; major increase in the microdeformations of the coating was also observed, particularly in these coatings obtained without saccharin.

The corrosion resistance of the deposits was first evaluated by observing the propagation of red rust on the deposits in the salt spray environment. For the passivated coatings the propagation of white rust was also observed. Table 2 shows the results obtained with both plating baths. It can be seen that the corrosion resistance of these alloys was very good, in spite of the microcracks observed on their surface. It has been speculated that the corrosion mechanism at this microcracked alloy surface might be compared to microcracked chromium: this minimizes the amount of corrosive attack over the metal surface through this network of microcracks. The addition of saccharin did not modify the appearance of white rust, but improved resistance to the red rust. The fissures observed in the cross section of some alloys obtained with this additive did not affect the corrosion results.

The electrochemical corrosion resistance of the coatings was measured using d.c. and a.c. methods. The results obtained using d.c. measurements (E_{corr}, R_p, i_{corr}) are summarized in Table 2. In contrast to observations made with zinc electrodeposits [15], here the electrochemical corrosion parameters were highly sensitive to the measurement conditions, being R_p and the anodic Tafel slopes the most affected factors. All the cathodic branches of the polarization curves showed a diffusion-dependent trend and, for non-passivated coatings, the anodic Tafel slopes were of about 30 mV, which agrees with other studies in chlorine-containing environments [23]. However, with the chromated deposits the anodic Tafel slope values were lower than those in the literature [24, 25] about 20 mV when measured after 3 h of immersion. This value increased up to 40/50 mV when the immersion time was increased or another measurement, such as cathodic polarization branch or an impedance measurement, was performed and then, the divergences might be accounted for by the different measurement recordings. To determine the corrosion rates, i_{corr} was calculated as usual using the Stern–Geary equation [26] with the lowest b_a value obtained in conditions where the system was least disturbed (after R_p determination using a potential interval of $E_{corr} \pm 5$ mV and only the potentiodynamic anodic scan).

The impedance plots (Fig. 8) obtained for these coatings were more complex than those observed in other cases for zinc–nickel alloys [27]. The Nyquist diagrams for the nonchromated deposits showed two capacitative loops with a complex response at very low frequencies. Initial studies conducted to find the equivalent circuit corresponding to this response showed that the second capacitative semicircle included a diffusion component. This component meant that the resistance values obtained from the impedance plots (R_{ac} in Table 2) were higher than those of R_p determined by d.c. measurements. For the chromated zinc–nickel alloys different capacitative and inductive elements were present (Fig. 9), but in any case diffusion components were observed. Here, it was observed that the R_p values were in accordance with the maximum resistance, but not with total resistance.

The presence of saccharin in the plating bath did not modify the electrochemical corrosion response, in

Table 2. Time (h) until the appearance of 1% of white and red rust and electrochemical corrosion parameters obtained for zinc–nickel alloys (Cr: passivated)

Plating bath	*W. rust* /h	*R. rust* /h	E_{corr} /mV	R_p /kΩ cm^2	b_a /mV	R_{ac} /kΩ cm^2	i_{corr} /μA cm^{-2}
Basic	–	800	−990	3.0	28	4.0	4.0
Basic + sacch.	–	900	−980	2.9	31	3.5	3.8
Basic (Cr)	550	1400	−985	78.0	15	79.0	0.1
Basic + sacch. (Cr)	525	1900	−975	79.0	18	80.0	0.1

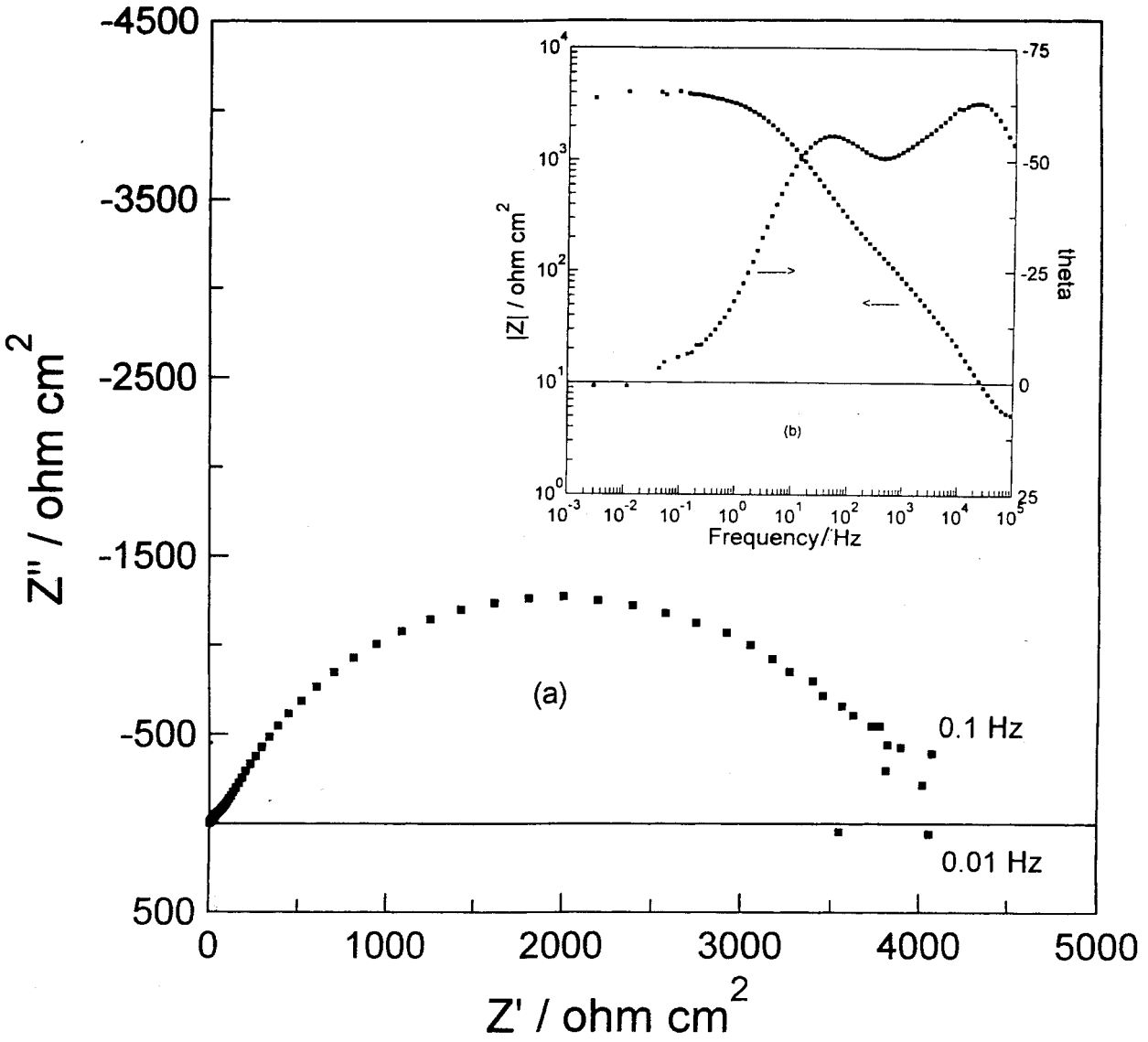

Fig. 8. Nyquist diagram (a) and Bode plots (b) obtained for nonpassivated Zn–Ni alloys.

agreement with the salt spray results, which indicated that this additive only affected the red corrosion response. Finally, although the electrochemical measurements with these Zn–Ni alloys were more sensitive than those observed in other cases, a correlation between salt-spray and electrochemical corrosion results could be established: coatings with R_p values higher than 35 kΩ cm^2 or i_{corr} lower than 0.4 μA cm^{-2} would pass industrial quality control (480 h before white corrosion in the fog chamber).

4. Conclusions

Zinc–nickel coatings obtained from an industrial bath were characterized by analysing several of their properties. It can be concluded that with the plating conditions used here, the alloys presented good appearance, a high corrosion resistance and microhardness and residual stress values at the usual level observed for zinc–nickel electrodeposits. Moreover, the structural study showed that no great changes were obtained in the interval of current densities used in a batch plating or when varying some of the electroplating parameters and then, the properties of the coatings were maintained over a wide interval of experimental conditions.

The influence of saccharin on deposit characteristics was also tested and it was observed that, in most cases, the additive only produced slight modifications to coating properties, although it improved corrosion resistance. When the concentration of Ni^{2+} was low, the mean effect of this additive was to promote the appearance of fissures on the coating layers closed to the substrate and a consequent decreases in microhardness and stress, but it did not modify corrosion behaviour. More work is needed to establish the origin of these fissures and their effect on other mechanical properties of the deposits.

Acknowledgements

The authors are grateful to the CICYT (project number MAT 94-1338) and to the Generalitat de Catalunya (SGR-67, 1996) for financial assistance, to

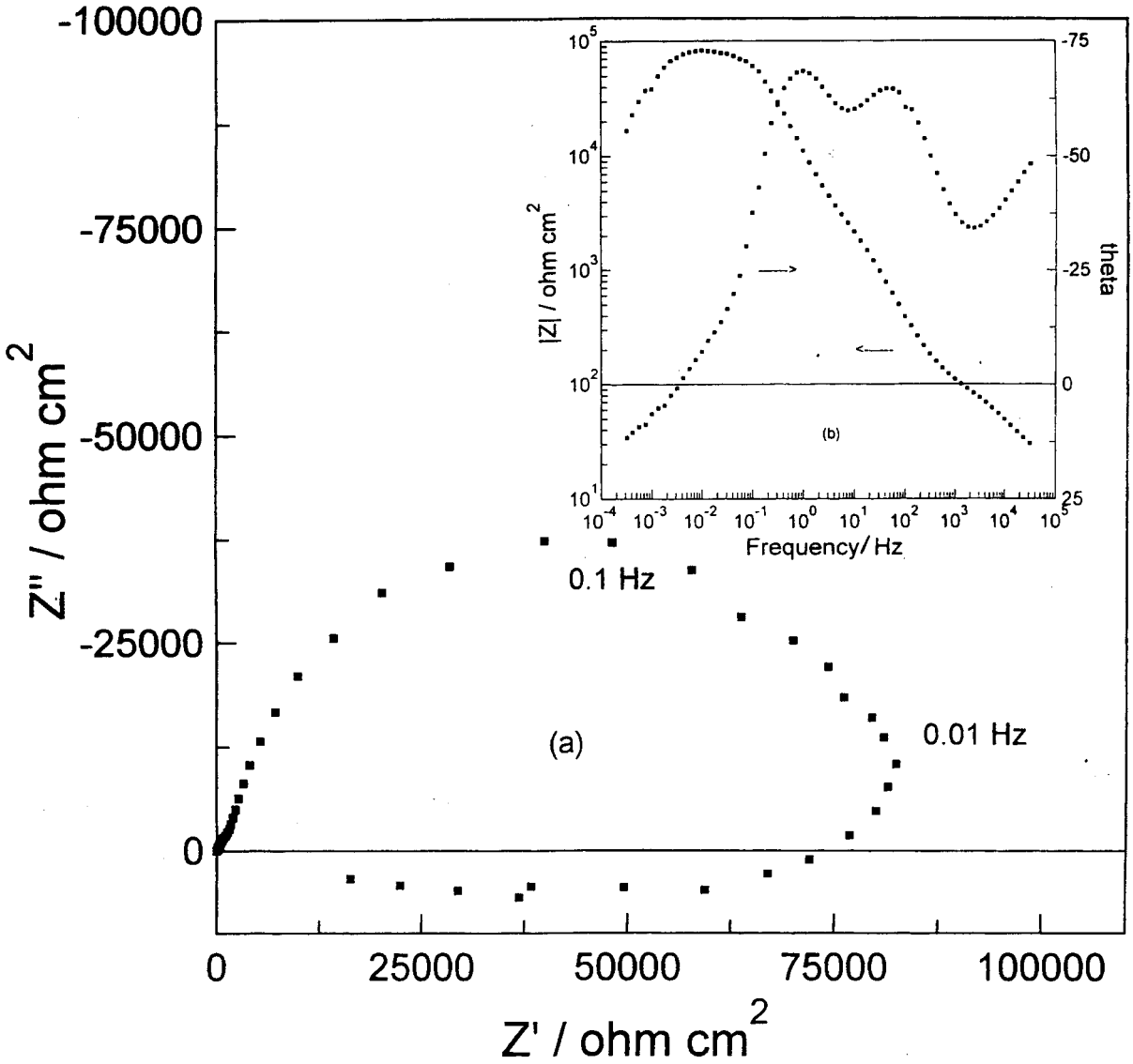

Fig. 9. Nyquist diagram (a) and Bode plots (b) obtained for passivated Zn–Ni alloys.

the Serveis Científico-Tècnics of the University of Barcelona for XRD measurements and, particularly, to X. Alcobé and J. Bassas for stress measurements. We thank the Ministerio de Educación y Ciencia for the financial support awarded to G.B.

References

[1] G. W. Loar, K. R. Romer and T. J. Aoe, *Plat. Surf. Finish.* **78** (1991) 74.
[2] J. Giridhar and W. J. Van Ooij, *Surf. Coat. Technol.* **52** (1992) 17.
[3] G. D. Wilcox and D. R. Gabe, *Corr. Sci.* **35** (1993) 1251.
[4] D. E. Hall, *Plat. Surf. Finish.* **71** (1983) 59.
[5] J. W. Dini and H. R. Johnson, *Met. Finish.* **77** (1979) 31.
[6] G. Ramesh Bapu, G. Devaraj, J. Ayyapparaju and R. Subramanian, *ibid.* **85** (1987) 49.
[7] L. Felloni, R. Fratesi, E. Quadrini and G. Roventi, *J. Appl. Electrochem.* **17** (1987) 574.
[8] R. Fratesi and G. Roventi, *ibid.* **22** (1992) 657.
[9] G. Barceló, J. García, M. Sarret, C. Müller and J. Pregonas, *ibid.* **24** (1994) 1249.
[10] J. I. Langford, *J. Appl. Cryst.* **11** (1978) 10.
[11] T. H. De Keijser, J. I. Langford, E. J. Mittemeijer and A. B. P. Vogels, *ibid.* **15** (1982) 308.
[12] I. C. Noyan and J. B. Cohen, 'Residual Stress. Measurement by Diffraction and Interpretation', Springer-Verlag, New York (1987).
[13] M. R. Lambert, R. G. Hart and H. E. Townsend, *SAE Tech. Pap. Series*, N. 831 817, Warrendale, PA (1983).
[14] T. Sasaki and Y. Hirose, *Thin Solid Films* **253** (1994) 356.
[15] G. Barceló, M. Sarret and C. Müller, *Electrochim. Acta*, **43** (1998) 13.
[16] F. Elkhatabi, M. Sarret and C.Müller, *J. Electroanal. Chem.* **404** (1996) 45.
[17] S. Swathirajan and Y. M. Mikhail, *J. Electrochem. Soc.* **136** (1989) 2188.
[18] C. V. Cooper and C. P. Beetz Jr, *Surf. Coat. Technol.* **47** (1991) 375.
[19] G. Sotirova, S. Sarnev and S. Armyanov, *Electrochim. Acta* **34** (1989) 1237.
[20] G. S. Sotirova-Chakarova and S. A. Armyanov, *J. Electrochem. Soc.* **137** (1990) 3551.
[21] R. Weil, G. J. Stanko and D. E. Moser, *Plat. Surf. Finish.* **63** (1976) 34.
[22] N. M. Martyak, *Surf. Coat. Technol.* **88** (1996) 139.
[23] L. M. Baugh, *Electrochim. Acta* **24** (1979) 657.
[24] L. Felloni, R. Fratesi and G. Roventi, 11th International Corrosion Congress, Florence (1990), Vol. 2, p. 2365.
[25] K. R. Baldwin, M. J. Robinson and C. J. E. Smith, *Corr. Sci.* **36** (1994) 1115.
[26] M. Stern and A. L. Geary, *J. Electrochem. Soc.* **104** (1957) 56.
[27] L. Fedrizzi, L. Ciaghi, P. L. Bonora, R. Fratesi and G. Roventi, *J. Appl. Electrochem.* **22** (1992) 247.